ACS OMEGA

http://pubs.acs.org/journal/acsodf

Article

Comparison of the Spectroscopically Measured Catalyst Transformation and Electrochemical Properties of Grubbs' First- and Second-Generation Catalysts

Marthinus R. Swart, Charlene Marais, and Elizabeth Erasmus*

Cite This: *ACS Omega* 2021, 6, 28642−28653

Read Online

ACCESS | Metrics & More | Article Recommendations | Supporting Information

ABSTRACT: According to UV−vis spectroscopy (0.10 mM, CH_2Cl_2 at 25 °C), the catalyst transformation (which could possibly include ligand dissociation with active catalyst formation, dimer formation, and decomposition) rate constants (k_{obs}) of Grubbs' first (**1**) and second (**2**) generation catalysts are 7.48 × 10^{-5} and 1.52 × 10^{-4} s^{-1}, respectively. From ^{31}P NMR (0.1 M, CD_2Cl_2, at 25 °C), the catalyst transformation was 5.1% for **1** and 16.5% for **2** after 72 h. However, due to the larger concentrations of the NMR samples compared to the UV−vis samples, the extent of transformation did not correspond. The oxidation potential of the Ru^{II}/Ru^{III} couple of **2** ($E^{o'}$ = 27.5 mV at ν = 200 mV s^{-1}) was considerably lower than that of **1** ($E^{o'}$ = 167 mV at ν = 200 mV s^{-1}). In the case of **1**, a second reduction peak appeared at slow scan rates. This may probably be ascribed to an electrochemically active compound that was formed from the intermediate cation $\mathbf{1}^{\bullet+}$ and the subsequent reduction of the latter. The oxidation/reduction of **1** proceeds according to an E_rC_i electrochemical mechanism (E_r = electrochemically reversible step, C_i = chemically irreversible step), whereas **2** proceeds according to an E_rC_r electrochemical mechanism (E_r = electrochemically reversible step, C_i = chemically reversible step).

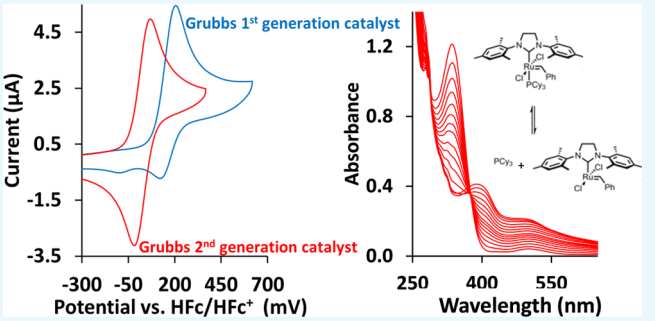

INTRODUCTION

Since the first reported Grubbs metathesis catalyst in 1992,[1] the field of ruthenium-based carbon−carbon bond formation reactions via metathesis methodology has gained considerable interest and continues to do so with its vast array of applications in cross-metathesis, self-metathesis, acyclic diene metathesis polymerization, ring-opening metathesis, ring-opening metathesis polymerization, ring-closing metathesis, asymmetric ring-closing metathesis, and ene−yne metathesis.[2−5] Testimony to this is the use of Grubbs' first- and second-generation catalysts as the catalysts of choice in the preparation of fine chemicals,[6−8] biologically active chemicals and drug fragments,[9−11] industrial applications,[7,12] polymer synthesis,[9,10] and polymer recycling.[13]

Since the first discovery of transition-metal-catalyzed metathesis in 1957,[14] various contributors in the field, including Bailey,[15] Banks,[15] Chauvin,[16] Fischer,[17] Maasböl,[17] and Schrock,[2,18−20] set the groundwork for metathesis reactions. When Robert Grubbs became active in this field, he focused his research on developing a more selective, more stable ruthenium-based metathesis catalyst, initially employing triphenylphosphine (PPh_3) as the coordinating ligand.[1,21,22] His endeavors to increase the activity of the catalyst by exchanging the triphenylphosphine ligands for tricyclohexylphosphine (PCy_3) ligands, along with simplifying the synthesis of the catalyst, led to the development of the now commercially available Grubbs first-generation catalyst, **1**.[1,3,23−25] Grubbs first-generation catalyst is a relatively stable ruthenium complex exhibiting a deformed square pyramidal crystal structure, with the apical position being occupied by the carbene carbon (see Figure 1 for the structure of **1**).[26,27]

Though this catalyst proved to be highly effective in the majority of metathesis-type reactions, it did show limitations in ring-closing metathesis and cross-metathesis of substrates with electron-withdrawing functional groups.[28] Subsequent investigations thus led to the design of the thermally more stable Grubbs second-generation catalyst, **2**. The ruthenium carbene complex **2** was obtained from the Grubbs first-generation catalyst by the substitution of one of the labile tricyclohexylphosphine groups with an *N*-heterocyclic carbene ligand (SIMes), which is a stronger net electron donor (see Figure 1 for the structure of **2**).[29−34] This strong σ-donation from the SIMes ligand along with its $\prod$−acceptor capacity greatly

Received: June 14, 2021
Accepted: September 23, 2021
Published: October 21, 2021

https://doi.org/10.1021/acsomega.1c03109
ACS Omega 2021, 6, 28642−28653

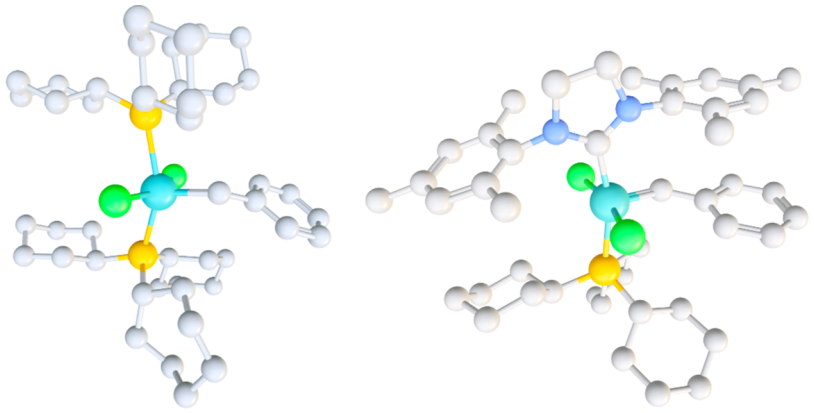

1 2

Figure 1. Optimized 3D structures of Grubbs' first (**1**) and second (**2**) generation catalysts. Hydrogen atoms are omitted for clarity.

increases the lability of the PCy_3 ligand in contrast to its unsaturated counterpart (IMes).[35] The $\prod-\prod$ stacking between the phenyl group of the SIMes ligand and the benzylidene carbene of **2** also further contributes to its greater stability.[36,37]

Various studies have recently been conducted, and investigations continue, to improve the Grubbs catalysts with regard to their activity, stability, catalyst lifetime, and selectivity.[38−42] These studies include DFT investigations,[43−48] ligand exchange research,[49−52] NMR investigations,[53−57] and mechanistic studies.[40,41,43,51] However, no comparative electronic study (UV−vis, electrochemical) on the valence and core electrons of Grubbs' first- or second-generation catalysts could be found. A few articles on the electrochemical behavior of ruthenium carbene complexes with structures similar to those of Grubbs' catalysts[58−64] report a one-electron Ru^{II}/Ru^{III} oxidation that may be reversible or irreversible, depending on the compound.[57,59,62,64] Investigations into the effect of different ligands on the electronic properties of the ruthenium center were anticipated to provide a feasible explanation for the slower initiation[65] and higher activity of **2** when compared to **1**.[23,63]

Herein, we therefore report on the characterization of the Grubbs first- and second-generation catalysts and the decomposition thereof by NMR, matrix-assisted laser desorption/ionization-time of flight mass spectrometry (MALDI−TOF MS), UV−visible spectroscopy (UV−vis), and attenuated total reflectance fourier transformed infrared (ATR−FTIR). Cyclic voltammetry (CV) is used to investigate the electrochemical character (and stability under potential variation) of these catalysts to obtain insight into the electronic properties of the valence electrons. UV−visible spectroscopy (UV−vis) provided information on the stability, whereas information on the extent of decomposition and the products of decomposition could be derived from ^1H and ^{31}P NMR experiments.

RESULTS AND DISCUSSION

Despite the enormous amount of research available on the catalytic behavior of Grubbs' first- and second-generation catalysts, few in-depth and comparative characterization studies on the catalysts itself are available.[26,34,66] The stability of the pre-catalyst as determined by UV−visible light spectroscopy in CH_2Cl_2, a solvent widely used in olefin metathesis reactions,[11,23,36] will thus be discussed. In addition, an electrochemical study employing cyclic voltammetry (CV), linear sweep voltammetry (LSV), and square wave voltammetry (SW), which gives insight into the valence electron properties under varied potentials, will be presented.

ATR−FTIR, UV−Visible, and NMR Spectroscopy. The ATR−FTIR spectra of **1** and **2** are, as expected, very similar, since the only difference between these catalysts is that one of the PCy_3 ligands in **1** is replaced with an SIMes ligand in **2** (see Table 1 and the Supporting Information for the ATR-FTIR figures). The major difference in the ATR−FTIR spectra is the C−N stretching frequency of the SIMes ligand, clearly visible at 1274 cm^{-1} for **2**, whereas it is absent for **1**. The C−P region shows two distinct stretching frequencies for **1** at 749 and 729 cm^{-1}, respectively, and only one frequency at 741 cm^{-1} for **2**.

Table 1. Summary of the UV−Vis and ATR−FTIR Spectral Data of 1 and 2[a]

	UV−vis data	kinetic data from UV−vis		IR data	
no	λ_{max} (nm); [ε (M^{-1} cm^{-1})]	k_{obs} (min^{-1})	k_{obs} (s^{-1})	ν_{P-C} (cm^{-1})	ν_{C-N} (cm^{-1})
1	334 [8750]; 514 [710]	4.5×10^{-3}	7.48×10^{-5}	749; 729	
2	334 [10 430]; 502 [590]	9.1×10^{-3}	1.52×10^{-4}	741	1274

[a]UV−Vis: Data of 0.10 mM solutions in dry CH_2Cl_2 for wavelengths at the absorption maxima (λ_{max}) and the extinction coefficients (ε) at these wavelengths. The observed rate constant (k_{obs}) at 334 nm for the catalyst transformation of **1** and **2** at 25 °C in CH_2Cl_2 under an Ar atmosphere. IR: Solid-state data of selected FTIR stretching frequencies.

The UV−vis absorption spectra of 0.10 mM solutions of **1** and **2** in dry CH_2Cl_2 at room temperature are shown in Figure 2, and the extracted data is summarized in Table 1. Both the Grubbs first (**1**) and second (**2**) generation catalysts gave strong absorbance bands at 334 nm, with the molar absorptivity, ε, of **1** (8750 M^{-1} cm^{-1}) being slightly lower than that of **2** (10 430 M^{-1} cm^{-1}). The band at 334 nm may be ascribed to the Ru−CHPh metal−ligand charge transfer (MLCT), in analogy to similar ruthenium benzylidenes.[67,68] Both catalyst species also showed weak absorption bands at longer wavelengths (514 and 502 nm for **1** and **2**, respectively).

https://doi.org/10.1021/acsomega.1c03109
ACS Omega 2021, 6, 28642−28653

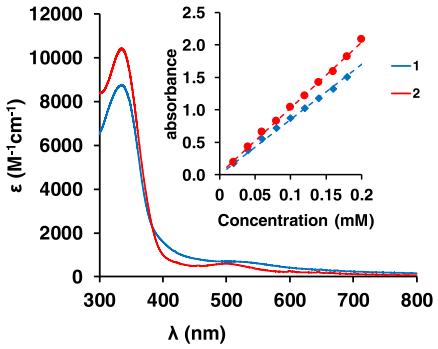

Figure 2. UV−vis spectra of 0.10 mM solutions of **1** (blue line) and **2** (red line) in dry CH_2Cl_2. Inset: Linear relationship between the absorbance and concentration for 1 (♦) and 2 (●) at λ = 334 nm, confirming the Beer−Lambert law for concentrations in the range 0.02−0.20 mM in dry CH_2Cl_2. Colors can be seen in the online version.

These can be attributed to the forbidden Ru=C_{ene} visible metal to ligand charge transfer (MLCT).[44,69,70] The blue shift observed in the visible MLCT band when one of the PCy_3 ligands in **1** is replaced with an SIMes ligand in **2** implies that the energy gap between the orbitals involved in the transfer is larger in **2** compared to **1**, and that the Ru=C_{ene} bond of **2** is thus weaker.[59] For this band, **1** also shows a slightly larger extinction coefficient (ε) of 710 M^{-1} cm^{-1} in comparison to 590 M^{-1} cm^{-1} for **2**, implying that the transition for **1** has a higher degree of allowedness.[71] Both Grubbs first- and second-generation catalysts followed the Beer−Lambert law, A = εCl, which implies a linear relationship between absorbance and concentration (see Figure 3 inset).

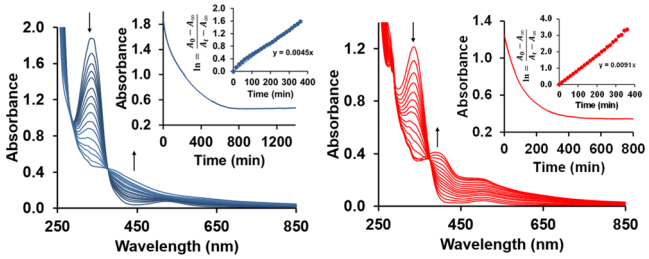

Figure 3. Overlaid UV−vis spectra measured for the dissociation of (left) **1**, blue graphs, and (right) **2**, red graphs, at different times at 25 °C using 0.10 mM solutions in dry CH_2Cl_2 under Ar. 1st Inset: Absorbance time trace at 334 nm. 2nd Inset: A first-order kinetic plot of the data for this process that leads to the observed rate constant, k_{obs}. For **1**, k_{obs} = 4.5 × 10^{-3} min^{-1} and for **2**, k_{obs} = 9.1 × 10^{-3} min^{-1}.

When Grubbs' catalysts **1** and **2** are dissolved in a suitable solvent, the phosphine (PCy_3) ligand dissociates during a slow kinetic process to eventually reach a dynamic equilibrium with the re-association of the phosphine[60] (see Scheme 1 for the reactions of **1** as an example (with additional transformations)).[72] This conversion of **1** and **2** in solution was studied by UV−vis spectroscopy. The experiments were conducted at 25 °C using 0.10 mM solutions of **1** and **2** in dry CH_2Cl_2 under Ar. The overlay spectra demonstrating the change in absorbance in the wavelength region 250−850 nm are shown in Figure 3, and the kinetic data are summarized in Table 1.

The dissociation of one of the phosphine ligands from **1** results in the formation of the 14-electron active catalytic species **1a** (Scheme 1), while dissociation of the only phosphine ligand from **2** creates **2a**, (SIMes)$RuCl_2$(CHPh). The observed catalyst transformation rate constant, k_{obs}, was found to be 7.48 × 10^{-5} s^{-1} for **1** and 1.52 × 10^{-4} s^{-1} for **2**, measured at λ = 334 nm (Table 1). The k_{obs} value of **2**, which is almost double that of **1**, was unexpected as the Grubbs group[73] reported the phosphine exchange for **2** to be two orders of magnitude slower than for **1** (^{31}P NMR: k_{obs} for the equilibrium reported as 9.6 s^{-1} for **1** and 0.13 s^{-1} for **2**, respectively, at 80 °C in toluene-d_8), and thus the initiation of **2** to be slower than that of **1**.[73] Though the dependence of phosphine exchange, and accordingly the active 14-electron species formation, on the temperature and solvent was expected,[33,34] the reversed k_{obs} trend most likely reflects phosphine exchange in addition to other catalyst transformation processes, e.g., dimerization.[63,74]

The ^{1}H and ^{31}P NMR spectra of the catalyst transformation [which could possibly include ligand exchange with active catalyst formation, dimer formation, and other decomposition reactions][63,78] were recorded after 72 h at 25 °C. In addition to the resonances of the pre-catalysts,[25,35,75,76] trace amounts of additional resonances appeared in the ^{1}H NMR spectra of both **1** and **2** (Figures S3 and S5). In the case of **1**, a new ^{31}P NMR resonance at δ_P 24.3 ppm, which was tentatively assigned to the 14-electron active catalytic species **1a**, was observed, though the major species was still pre-catalyst **1** (δ_P 36.05 ppm) (see Figure 4 and Figure S4 for the ^{31}P NMR of **1** after 72 h).[77] Pre-catalyst **2** (δ_P 29.19 ppm) was also the major phosphorus-containing species in the reaction mixture of **2** (Figure S6). No trace of free PCy_3 (δ_P 10.5 ppm)[78] could be observed in the reaction mixtures of either **1** or **2**, but a resonance at δ_P 49.7 ppm, which could be ascribed to tricyclohexylphosphine oxide (O=PCy_3) in correlation with the published value,[79] confirmed the dissociated phosphine to be oxidized. This oxidation may be ascribed to the presence of trace amounts of adventitious oxygen in the reaction mixture despite our best efforts to keep the conditions inert (as was also reported by other groups).[78,80,81] By trapping the dissociated PCy_3,[80] oxygen may thus shift the equilibrium between the pre-catalyst and active species towards the latter (Scheme 1).[102] As the active catalyst species **2a** does not have a coordinated phosphine ligand, no extra resonances appearing upfield of **2** were expected nor observed in the ^{31}P NMR spectrum of the reaction mixture of **2** (see Figure S6 in the Supporting Information). Another resonance appeared at δ_P 34.9 ppm in the ^{31}P NMR spectrum of the reaction mixture of **1** (Figure 4). This resonance was tentatively ascribed to possible dimerization,[34,63,82−85] though other decomposition products cannot be excluded.[74] The tentative assignment of the ^{31}P NMR resonances at δ_P 24.3 and 34.9 ppm to the active catalytic species **1a** and a possible dimeric species (**1b**), respectively, is supported by the observation of a molecular ion with m/z 542, which may be ascribed to the molecular ions $[M_{1a}]^+$ and/or $[M_{1b}]^{2+}$, by MALDI−TOF MS (Figure S8). Bimolecular coupling of the 14-electron active species **1a** and **2a** could furthermore be confirmed in an indirect way by the observation of the bimolecular decomposition product, (*E*)-stilbene (**3**)[74,102] (δ_H 7.14 ppm, s, =CH), in the reaction mixtures after 72 h (Figure S7). The cycloaddition of oxygen to the 14-electron species was furthermore confirmed by the presence of benzaldehyde (**4**) (δ_H 10.01 ppm, s, CHO and 7.88 ppm, d, J = 7.5 Hz, H-2 and H-6) in the reaction mixtures after 72 h (Figure S7). The formation of these species may be

https://doi.org/10.1021/acsomega.1c03109
ACS Omega 2021, 6, 28642−28653

Scheme 1. Schematic Representation of the Phosphine Dissociation/Association Equilibrium of 1 to Form the Active Catalytic Species 1a, Followed by Phosphine Oxidation and Decomposition of 1a

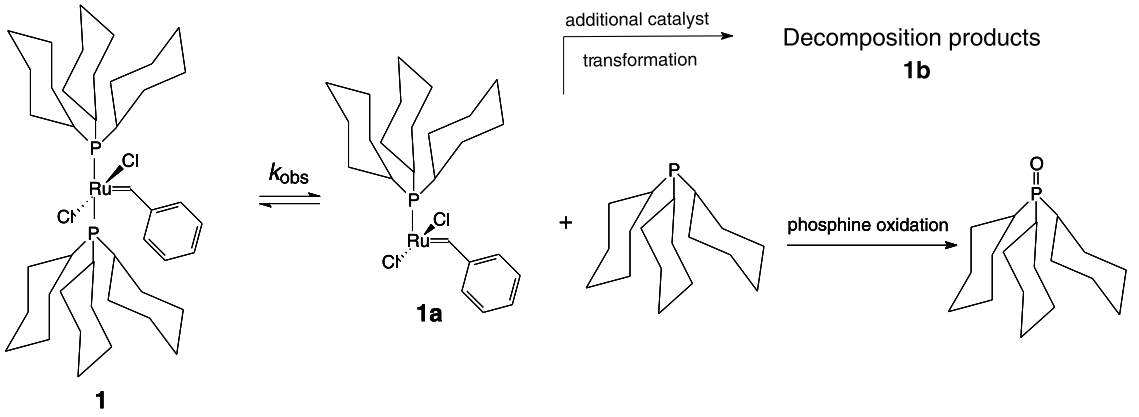

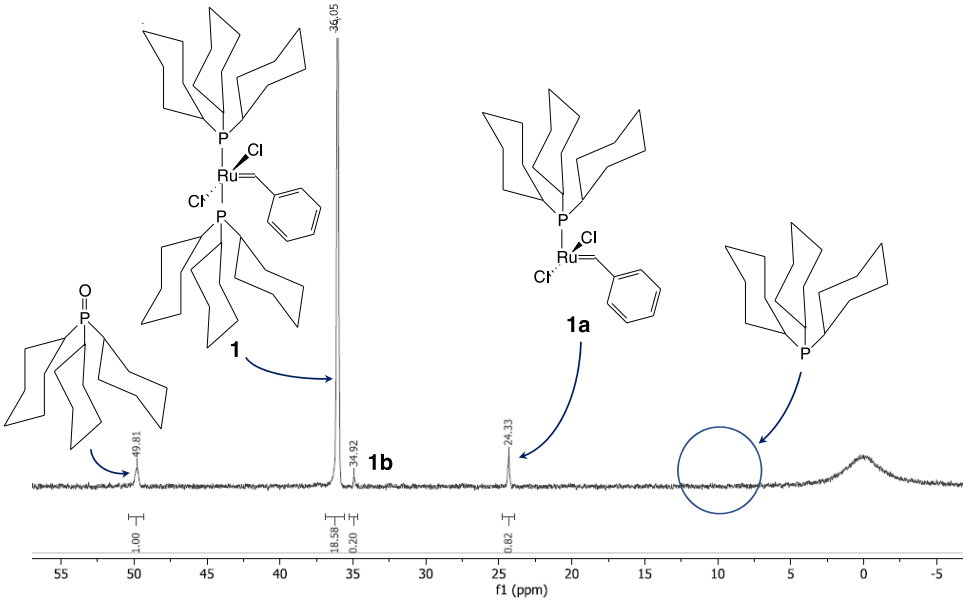

Figure 4. ^{31}P NMR of **1** after being dissolved in CD_2Cl_2 at 25 °C for 72 h, indicating the assigned structures.

explained by the decomposition pathways suggested by Ton and Fogg[96] in the presence of oxygen (Scheme 2). For more information on the decomposition of ruthenium-based metathesis catalysts, the reader is referred to a recent review by Jawiczuk, Marczyk, and Trzaskowski.[74]

The integral ratio of the ^{31}P NMR resonances of O=$\underline{P}Cy_3$ ($\int$ = 1.00) to **1a** + **1b** ($\int$ = 0.82 + 0.20) is 1: 1 (Figure 4). Thus, under our conditions, each PCy_3 ligand that dissociated from **1** to form the active species **1a** and an additional species **1b** [**1b** most probably corresponds to the dimeric **1b** in Scheme 2, but other decomposition products cannot be ruled out] seems to be oxidized to O=PCy_3 by trace amounts of adventitious O_2. Furthermore, from the integral ratios of O=PCy_3 versus **1** or **2**, 5.1% PCy_3 dissociation was observed for **1** and 16.5% for **2** after 72 h at 25 °C in CD_2Cl_2.[i] The small transformation percentage is also reflected in the small signal to noise ratios of the additional resonances in the ^1H NMR spectra of **1** and **2** after 72 h (*vide supra*).

As expected, the extent of transformation of the pre-catalysts in the UV−vis and NMR experiments did not correspond due to the concentration differences (0.1 mM and 0.1 M in the UV−vis and NMR experiments, respectively). The large difference in concentration was inevitable due to the inherent requirements of each technique; low concentrations give poor signal to noise ratios in NMR experiments, whereas UV−vis requires low concentrations for the analyte to obey the Beer−Lambert law. To directly compare the results, a 0.1 M sample of **1** was prepared in CH_2Cl_2 and incubated at 25 °C. After 72 h, the sample was diluted to 0.1 mM and the UV−vis spectrum collected (with little time elapse). The absorbance of this sample corresponded to that of the 0.1 mM reaction mixture after *ca.* 1 h, implying that equilibrium has not been reached yet (Figure S10). This finding confirms that concentration is a very important factor in the rate of transformation. Though the reaction with oxygen was reported to be slower than PCy_3 dissociation, the oxygen concentration is another factor to be considered as van der Westhuizen et al. reported the rate of reaction between the Grubbs first-generation catalyst and oxygen to be first order in oxygen.[81] This aspect will be the topic of a follow-up paper.

Electrochemistry. The electrochemical properties of the Grubbs first- and second-generation catalysts (**1** and **2**) were investigated in dry CH_2Cl_2 at both 5 and 25 °C with

https://doi.org/10.1021/acsomega.1c03109
ACS Omega 2021, 6, 28642−28653

Scheme 2. Proposed Oxidative Decomposition of the Grubbs First (1) and Second (2) Generation Catalysts

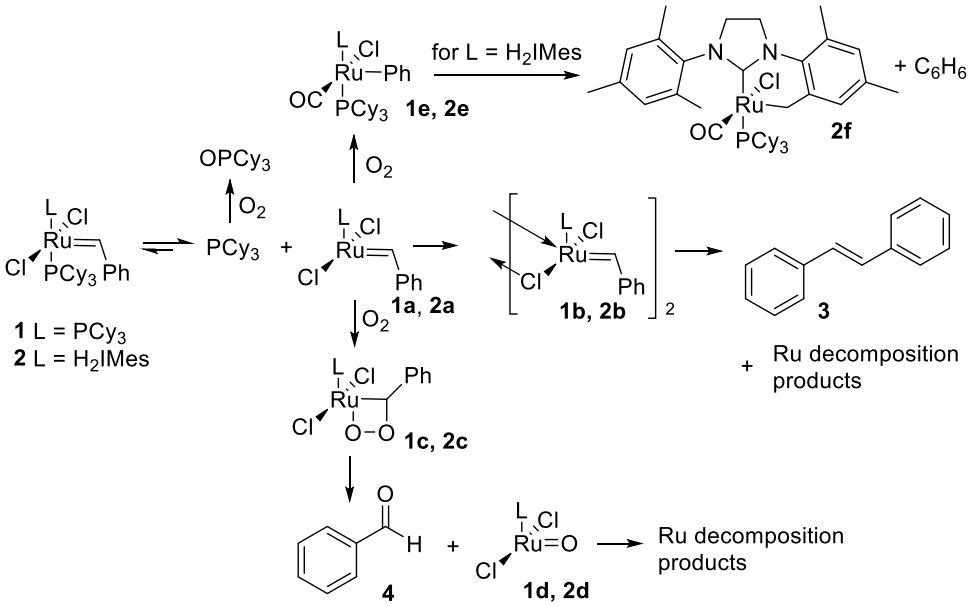

$[N(^{n}Bu)_4][PF_6]$ as the supporting electrolyte and under a blanket of argon.

Figure 5 shows the cyclic voltammograms (CVs) of **1** at 25 °C and scan rates ranging from 20 to 2000 mV s^{-1}. Data that can be extracted from the CVs in Figure 5 are summarized in Table 2.

A single ruthenium-based oxidation process (O1/R1) was observed for **1**, which was confirmed by square wave voltammetry (SW) (Figure 5). The linear sweep voltammetry (LSV) showed that the number of electrons transferred during the oxidation process, O1, is comparable with the number of electrons transferred for the same concentration (*ca.* 0.8 mM) of Fc* in solution (Figure 5). Thus, during the oxidation process O1, one electron is transferred from **1**, thus confirming the involvement of the Ru^{II}/Ru^{III} couple.

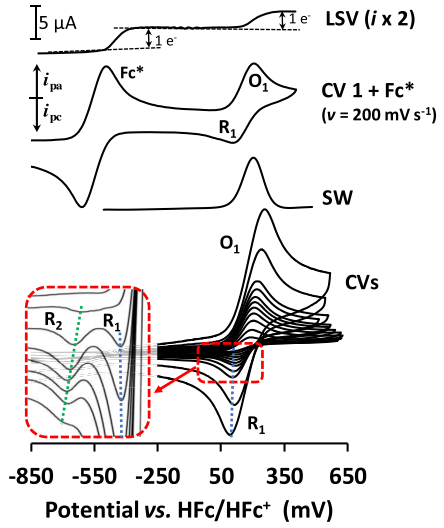

Figure 5. Top to bottom: Linear sweep voltammogram (LSV) at 25 °C in the presence of 0.1 mol dm^{-3} $[N(^{n}Bu)_4][PF_6]$ as supporting electrolyte at a scan rate of 2 mV s^{-1} of 0.8 mM **1** and 0.8 mM Fc*(Fc* = decamethylferrocene as internal standard). Cyclic voltammograms of 0.8 mM CH_2Cl_2 solutions of **1** and 0.8 mM Fc* at a scan rate of 200 mV s^{-1}. Square wave (SW) voltammogram of **1** at 15 Hz. Cyclic voltammograms of 0.8 mM CH_2Cl_2 solutions of **1** at 25 °C in the presence of 0.1 mol dm^{-3} $[N(^{n}Bu)_4][PF_6]$ as supporting electrolyte at scan rates of 20 (smallest current), 50, 100, 150, 200, 250, 300, 400, 500, 1000, and 2000 (largest current) mV s^{-1}. Inset: Enlargement of the area in the red dotted line; potential −300 to 300 mV and current 0 to −1 μA. Colors can be seen in the online version.

Theoretically, ΔE = 59 mV for a reversible one-electron transfer during an electrochemical process.[86] However, under our conditions, decamethylferrocene, Fc* (the internal standard), exhibited 77 < ΔE < 93 mV, denoting the range of electrochemical reversibility. For an electron transfer process to be deemed chemically reversible, i_{pc}/i_{pa} = 1.[87]

Varying the scan rate between 20 and 2000 mV s^{-1} indicated that the electrochemical behavior of **1** is not reproducible. When the CVs were recorded at fast scan rates (v > 500 mV s^{-1}), the oxidation wave Ru^{II}/Ru^{III} approached chemical reversibility (with i_{pc}/i_{pa} = 0.98, for v = 2000 mV s^{-1}), but was electrochemically irreversible (ΔE_p = 166 mV for v = 2000 mV s^{-1}). However, upon decreasing the scan rate, an additional reduction peak R2 appeared and the oxidation wave of **1** (denoted by O1 and R1) became chemically irreversible (i_{pc}/i_{pa} < 1, i_{pc}/i_{pa} = 0.34, for v = 100 mV s^{-1}), but electrochemically reversible ($\Delta E_p \leq$ 91 mV) (Table 2).

This behavior is consistent with an E_rC_i electrochemical mechanism (E_r = electrochemically reversible step, C_i = chemically irreversible step)[88,89] followed by another electrochemical process. In this mechanism, the oxidized product $\mathbf{1}^{\bullet+}$ formed during the oxidation process O1 (Figure 5) is reversibly reduced (peak R1) to regenerate **1**, but $\mathbf{1}^{\bullet+}$ also slowly and irreversibly undergoes a chemical reaction to form **X** (eq 1). This newly formed species (**X**) has a lower reduction potential than that of $\mathbf{1}^{\bullet+}$ (R1) and gave rise to the reduction peak R2. This chemical reaction was slower than the CV time scale at fast scan rates, and accordingly, R2 could not be detected for scan rates larger than 500 mV s^{-1}. The electrochemical scheme in eq 1 is consistent with the electrochemical behavior of **1**.

It is well known that an electrochemically generated species (like $\mathbf{1}^{\bullet+}$) can interact with the surrounding ionic medium. The

https://doi.org/10.1021/acsomega.1c03109
ACS Omega 2021, 6, 28642−28653

Table 2. Cyclic Voltammetry Data of 0.8 mmol dm^{-3} Solutions of 1 and 2 in CH_2Cl_2 Containing 0.1 mol dm^{-3} $[N(^nBu)_4][PF_6]$ as Supporting Electrolyte at 25 and 5 °C[a]

Grubbs' first-generation catalyst, **1**									
25 °C								5 °C	
v (mV s^{-1})	E_{pa}[b] (mV)	$E^{o,b}$ (mV)	ΔE_p[b] (mV)	i_{pa} (μA)	i_{pc} (μA)	i_{pc}/i_{pa}[c]	$E_{pc\ R2}$[b] (mV)	i_{pa} (μA)	i_{pc}/i_{pa}[c]
20	191			1.84				1.74	
50	200			2.88			−45	3.07	
100	204	165	77	3.91	1.32	0.34	−82	3.49	0.56
150	207	166	82	5.18	1.84	0.36	−97	4.00	0.57
200	209	167	84	5.64	2.19	0.39	−109	4.51	0.57
250	211	168	86	6.33	2.76	0.44	−110	4.61	0.58
300	216	169	93	7.02	3.22	0.46	−108	4.92	0.65
400	223	168	111	7.71	4.26	0.55	−117[d]	5.85	0.66
500	224	166	116	8.48	5.06	0.60	−122[d]	6.15	0.68
1000	241	178	126	12.74	11.90	0.74		7.82	0.73
2000	259	176	166	17.42	17.03	0.98		13.15	0.86
Grubbs' second-generation catalyst, **2**									
25 °C								5 °C	
20	61	26	70	1.80	1.73	0.96	0.67	1.00	
50	64.5	26.5	76	2.79	2.65	0.95	0.97	1.00	
100	65.5	27	77	3.42	3.24	0.95	1.34	1.00	
150	69	27.5	83	4.05	3.78	0.93	1.64	0.98	
200	69.5	27.5	84	4.95	4.55	0.92	1.87	0.98	
250	73	27.5	91	5.08	4.62	0.91	2.16	0.97	
300	69.5	29.5	80	5.07	4.56	0.90	2.39	0.97	
400	79.5	29.5	100	6.17	5.34	0.88	2.61	0.97	
500	81.5	29	105	6.86	6.03	0.88	3.00	0.95	
1000	90	34	112	7.46	6.56	0.88	4.15	0.91	
2000	105	36	138	10.44	9.08	0.87	5.72	0.88	

[a]Scan rate = 20−2000 mV s^{-1}, potentials referenced *vs* FcH/FcH$^+$. [b]All potentials are referenced against FcH/FcH$^+$ at 0.00 mV. [c]Peak current ratios are always $(i_{reverse\ scan})/(i_{forward\ scan})$. [d]Estimates only as values of $E_{pc\ 2}$ cannot accurately be determined.

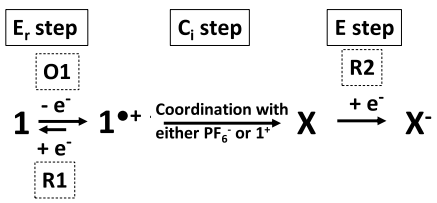

CH_2Cl_2 used as solvent for the electrochemical medium is a poorly coordinating solvent;[48] thus, unlike CH_3CN, which is known to coordinate with electrochemically generated species such as bis(cyclopentadienyl)ruthenium(II)-containing β-diketones to produce $[(RCOCH_2COC_5H_4)(C_5H_5)Ru^{IV}\text{-}CH_3CN]^{2+}$),[90] the chemical reaction following the oxidation of **1** cannot be ascribed to the coordination of $\mathbf{1}^{\bullet+}$ with CH_2Cl_2. However, the chemical reaction following the

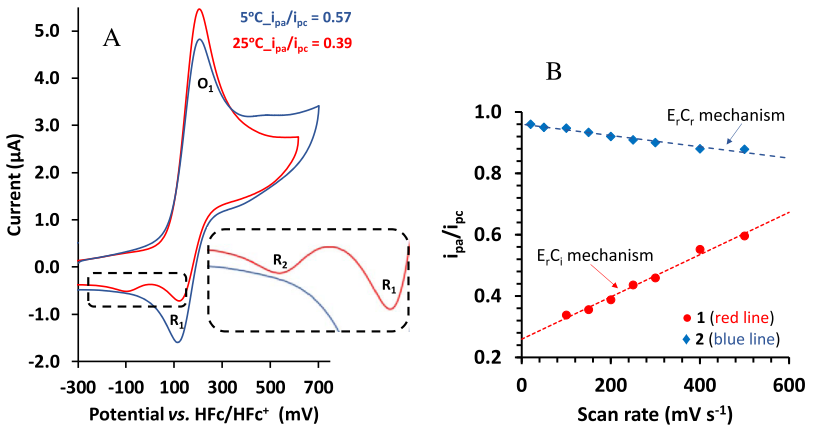

Figure 6. (A) Cyclic voltammograms of a 0.8 mM CH_2Cl_2 solution of **1** at 5 °C (blue line) and 25 °C (red line) in the presence of 0.1 mol dm^{-3} $[N(^nBu)_4][PF_6]$ as the supporting electrolyte at a scan rate of 200 mV s^{-1} under an argon atmosphere. Inset: Enlargement of the area in the dotted line; potential *ca.* −270−100 mV and current *ca.* −0.2 to −0.8 μA. (B) Relationships between i_{pc}/i_{pa} and scan rates at 25 °C have a positive slope for the E_rC_i mechanisms, as shown for **1** (● red line), or a negative slope for E_rC_r mechanisms, as shown for **2** (♦ blue line). Colors can be seen in the online version.

https://doi.org/10.1021/acsomega.1c03109
ACS Omega 2021, 6, 28642−28653

oxidation of **1** in all likelihood entails the formation of an ion pair with the electrolyte (the PF_6^-) or an electrochemically active decomposed Ru-species, or the coordination of $\mathbf{1}^{\bullet+}$ with another radical cation, $\mathbf{1}^{\bullet+}$, i.e., dimerization to a dimeric species (**X**). The latter is in correlation with the electrochemical behavior of ruthenocene, which forms a dication $[(Ru(C_5H_5)_2)_2]^{2+}$[91,92] upon oxidation of the Ru^{II}. It would be tempting to assign the reduction peak R2 observed in the CV of **1** (Figures 6 and 7) to the reduction of a dimeric species of **1**. However, this would require further experimental data, which is currently not available.

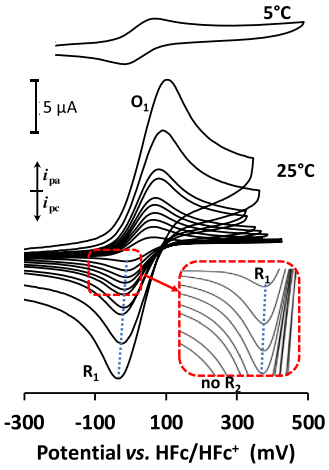

Figure 7. Top: 200 mV s^{-1} cyclic voltammogram of a 0.8 mM CH_2Cl_2 solution of **2** at 5 °C in the presence of 0.1 mol dm^{-3} $[N(^nBu)_4][PF_6]$ as the supporting electrolyte at a scan rate of 200 mV s^{-1}. Bottom: Cyclic voltammograms of a 0.8 mM CH_2Cl_2 solution of **2** at 25 °C in the presence of 0.1 mol dm^{-3} $[N(^nBu)_4][PF_6]$ as the supporting electrolyte at scan rates ranging from 20 (smallest current) to 2000 (largest current) mV s^{-1}. Inset: Enlargement of the area in the red dotted line; potential −110 to 50 mV and current 0 to −3 μA. Colors can be seen in the online version.

Figure 6 shows the cyclic voltammograms of **1** at 5 °C (blue line) and 25 °C (red line) measured at a scan rate of 200 mV s^{-1} (additional CVs of 1 at 25 and 5 °C are given in Supporting Information). The temperature of 5 °C is sufficiently low to slow the kinetic process of the formation of X down to a point where R2 is not prominently observed, but only the reduction of $\mathbf{1}^{\bullet+}$ back to 1. A similar retarding effect on a secondary reaction due to slower kinetics at decreased temperature has been reported for the conversion of a ruthenocene dimer to a dinuclear Ru-complex.[89]

Grubbs' second-generation catalyst, **2**, also only shows a one-electron transfer process (Table 2 and Figure 7) (the LSV, SW, and more CVs at 5 and 25 °C are provided in the Supporting Information). The O1/R1 process is electrochemically reversible at scan rates < 400 mV s^{-1}, with $\Delta E_p \leq 93$ mV. The reduction peak of the Ru^{II}/Ru^{III} oxidation wave of **2** only shows one peak (at 5 and 25 °C), unlike **1**.

The Ru^{II} in **2** exhibited a completely opposite trend to the current ratios displayed by **1**. At slow scan rates, the i_{pc}/i_{pa} ratios of **2** approach **1** and therefore show chemical reversibility. Conversely, the faster the scan rate, the less chemically reversible the electron transfer of the Ru^{II}/Ru^{III} couple. This implies that the electrochemically oxidized species, $\mathbf{2}^{\bullet+}$, is chemically converted (via an equilibrium reaction) into an electrochemically inactive species (no additional oxidation or reduction peaks were detected within the CV window, or these peaks are outside the solvent potential window).[91] As a result, it can be deduced that when the scan rate is slow, $\mathbf{2}^{\bullet+}$ is regenerated fast enough from the chemically formed product to allow i_{pc}/i_{pa} ratios to approach unity. However, at fast scan rates, $\mathbf{2}^{\bullet+}$ cannot be regenerated fast enough to produce $i_{pc}/i_{pa} \approx 1$, and hence the current ratio deviates further and further from unity. If given enough time, even at fast scan rates, all chemically transformed products will eventually convert back to $\mathbf{2}^{\bullet+}$, but not before the peak cathodic potential is reached during the reverse scan. This behavior describes an E_rC_r electrochemical mechanism (E_r = reversible electrochemical step; C_r = reversible chemical step)[86,93] and may be represented by the electrochemical Scheme in eq 2.

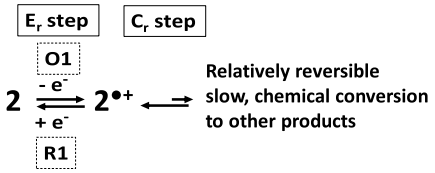

The easiest way to distinguish between the E_rC_i mechanism seen for **1** and the E_rC_r mechanism seen for **2** is by plotting the graphs of i_{pc}/i_{pa} against the scan rates.[87] A linear relationship with a negative slope is representative of an E_rC_r mechanism and a linear relationship with a positive slope between these quantities is representative of an E_rC_i mechanism (Figure 7B). The results summarized in eqs 1 and 2 are consistent with **2** being electrochemically more stable than **1**.[27]

The formal oxidation potential, $E^{\circ\prime}$, of **2** ($E^{\circ\prime}$ = 27 mV at v = 100 mV s^{-1}) is lower than that of **1** ($E^{\circ\prime}$ = 165 mV at v = 100 mV s^{-1}), indicating that it is easier to oxidize **2** than **1**. This shows that the Ru^{II} center in **2** is more electron rich than that in **1**, and that the SIMes ligand offers additional stabilization to $\mathbf{2}^{\bullet+}$. It also offers another possible explanation as to why **2** has a higher catalytic activity towards metathesis than **1**,[50] since it is easier for the valence electrons to participate in electron transfer. This deduction is furthermore corroborated by the blue shift in the visible MLCT band of **2** compared to **1**, with the larger energy gap being consistent with a weaker $Ru{=}C_{ene}$ bond (*vide supra*).

To investigate the intrinsic electrochemical stability of **1** and **2**, multiple cyclic voltammogram segments were measured consecutively at 25 °C and 200 mV s^{-1}. The multiple segment CVs of **1** are shown in Figure 8, and for **2** they are shown in the Supporting Information, Figure S16. For **1**, a slight decrease in current and an escalation of the oxidation potential were observed for the first 20 segments (10 complete cycles), which may be ascribed to the electrochemical instability of **1**. However, this is followed by an increase in current (and a further escalation in oxidation potential) as the number of segments increase. This may be due to the formation of a new species. A 175 mV shift of the E_{pa} to 431 mV is seen after 50 cycles (100 segments). **2** is moderately more electrochemically stable than **1**, since the E_{pa} only displays a 74 mV shift (new E_{pa} = 143.5 mV) to higher potentials, with a small decrease in current.

A summary of the properties of **1** and **2** reported in this article, as well as relevant reported data, is presented in Table 3 for comparison.

https://doi.org/10.1021/acsomega.1c03109
ACS Omega 2021, 6, 28642−28653

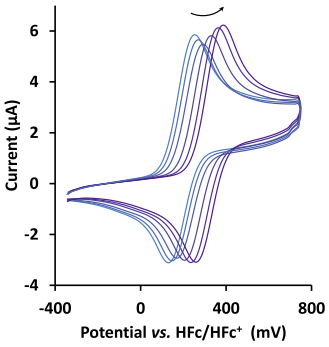

Figure 8. Consecutive cyclic voltammogram segments of the 0.8 mM CH_2Cl_2 solution of **1** at 25 °C in the presence of 0.1 mol dm^{-3} $[N(^nBu)_4][PF_6]$ as the supporting electrolyte at a scan rate of 200 mV s^{-1} under an argon atmosphere. Only segments 5/6, 11/12, 33/34, 47/48, and 61/62 are shown; CVs showing all cycles are shown in the Supporting Information (Figure S15).

CONCLUSIONS

According to UV−vis kinetics, catalyst **2** with the SIMes ligand is less stable in CH_2Cl_2 at 25 °C than catalyst **1** with two PCy_3 ligands (k_{obs} of 1.52×10^{-4} and 7.48×10^{-5} s^{-1} for **2** and **1**, respectively). This observation was confirmed by ^{31}P NMR, according to which 16.5% catalyst transformation was observed for **2** after 72 h as compared to 5.1% for **1**. However, due to the large concentration difference between the NMR and UV−vis samples, the extent of transformation was also different. The k_{obs} values cannot be ascribed to pure phosphine exchange and thus the formation of the active 14-electron species (due to additional peaks being observed in the ^{31}P NMR), but may also include dimer formation and/or decomposition.

Cyclic voltammetry revealed that both **1** and **2** are involved in Ru^{II}/Ru^{III} one-electron transfer processes, with **2** being oxidized at much lower potentials than **1**. This indicates that the SIMes ligand (in **2**) is more electron-donating than the PCy_3 ligand (in **1**), and consequently that the Ru(II) center in **2** is more electron rich than the Ru(II) center in **1**.

However, electrochemical reduction in the solution phase (CH_2Cl_2) of the radical cations $\mathbf{1}^{\bullet+}$ and $\mathbf{2}^{\bullet+}$ proceeds very differently. At slow scan rates, two reduction peaks were observed for $\mathbf{1}^{\bullet+}$. The oxidation/reduction of **1** proceeds according to an E_rC_i electrochemical mechanism, followed by another electrochemical process of the newly formed species. This newly formed species is most probably a dimer formed between two $\mathbf{1}^{\bullet+}$ species. The oxidation/reduction of **2** proceeds according to an E_rC_r electrochemical mechanism. At faster scan rates, the electron transfer of **2** becomes

Table 3. Summary of the Properties of GI and GII (UV−Vis Data, Kinetic Data, NMR, and CV) from This Study as Well as from Other Reports

	UV−vis data			kinetic data (PCy_3 dissociation/decomposition)			
	λ_{max} (nm)	solvent	ref	k_{obs} (s^{-1})	additive	solvent	ref
GI	334	CH_2Cl_2	[a]	7.48×10^{-5}	adventitious O_2	CH_2Cl_2 (25 °C)	[a]
	∼336	toluene	66	9.6	PR_3	toluene (80 °C)	73
GII	330	CH_2Cl_2	[a]	1.52×10^{-4}	adventitious O_2	CH_2Cl_2 (25 °C)	[a]
	∼337	toluene	66	0.13	PR_3	toluene (80 °C)	73
	337	DCE	94	1.7×10^{-5}	O_2	CH_2Cl_2 (25 °C)	80
	330	CH_2Cl_2	95				

	^{31}P NMR δ (ppm)				^1H NMR		
	1 or 2	**1a or 2a**	**decomposition products**	$O=PCy_3$	δ (ppm) alkylidene	solvent	ref
GI	36.05	24.4	34.9	49.7	20.02	CD_2Cl_2	[a]
	30.63					CD_2Cl_2	25
					19.56	C_6D_6	25
	∼35.5	∼24.5	∼32.4	∼49.8	19.93	$CDCl_3$	66
GII	29.19	21.2		49.65	19.1	CD_2Cl_2	[a]
	∼28.8				∼19.14	$CDCl_3$	66
	27.2					THF	69
	30.13		26.23,[b] 32.6[c]	48.35		toluene	96
					18.94	CD_2Cl_2 (−40 °C)	8
					19.12	$CDCl_3$	4

	electrochemistry (cyclic voltammetry)						
	E_{pa} (mV)	$E^{o'}$ (mV)	ΔE_p (mV)	i_{pc}/i_{pa}	referenced against	solvent system	ref
GI	209	167	84	0.39	HFc/HFc$^+$	$CH_2Cl_2/[N(^nBu)_4][PF_6]$	[a]
	739	181	∼167	∼0.41	Ag/AgCl	$CH_2Cl_2/[N(^nBu)_4][PF_6]$	66
		700	130		SCE	CH_2Cl_2/TEAP	97
GI-Fc(a)[d]		84	100		SCE	CH_2Cl_2/TEAP	10
GI-Fc(b)[e]		88	140		SCE	CH_2Cl_2/TEAP	10
GII	69.5	27.5	84	0.92	HFc/HFc$^+$	$CH_2Cl_2/[N(^nBu)_4][PF_6]$	[a]
	702	554	∼297	∼0.94	Ag/AgCl	$CH_2Cl_2/[N(^nBu)_4][PF_6]$	66

[a]Data from this work. [b]**2e**. [c]**2f**. [d] 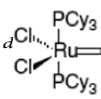 . [e] 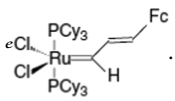 .

https://doi.org/10.1021/acsomega.1c03109
ACS Omega 2021, 6, 28642−28653

increasingly less chemically reversible. This is due to a relatively reversible, but slow, chemical conversion to other products. At slower scan rates, $2^{\bullet+}$ could be chemically regenerated from the unknown product(s) to be reduced back to **2**.

Both **1** and **2** behave electrochemically reversible at slow scan rates. **2** is chemically more stable than **1** at slow scan rates, whereas **1** is chemically more stable than **2** at fast scan rates. Furthermore, **2** is electrochemically more stable than **1** with repeated cycling of the potential.

The influence of the slightly different electron-donating properties of the SIMes and PCy_3 ligands is more pronounced on the electrochemical properties (valence electrons) of **1** and **2** than on the photoemission properties (core electrons) thereof.

EXPERIMENTAL SECTION

General. The Grubbs first-generation catalyst [benzylidene-bis(tricyclohexylphosphino)-dichlororuthenium], **1**, Grubbs second-generation catalyst [1,3-bis(2,4,6-trimethylphenyl)-2-imidazolidinylidene)dichloro(phenylmethylene)-(tricyclohexylphosphino)ruthenium], **2**, and other solid reagents and solvents used in this study were purchased from Sigma-Aldrich and were used without further purification. Solvents were dried through a small column of activated neutral alumina (10% v/v) prior to use. All of the preparations were carried out under Schlenk conditions or in a glovebox.

Spectroscopic Characterization Techniques. *Attenuated Total Reflectance Fourier Transform Infrared (ATR−FTIR) Spectroscopy.* Solid-state ATR−FTIR spectra were recorded using a Thermo Scientific IR spectrometer with a Nicolet iS50 ATR attachment. UV−visible (UV−vis) spectra were recorded on 0.02−0.20 mM solutions in dry dichloromethane (CH_2Cl_2) under an argon atmosphere using a Shimadzu UV-1800 UV/Visible spectrophotometer. A 2 mL quartz cuvette with a path length of 1 cm was used. UV−vis stability investigations over time (24 h) were conducted on 0.1 mM solutions of **1** and **2** in dry dichloromethane (CH_2Cl_2) under an argon atmosphere at 25 °C. Spectra were recorded every 15 min throughout the 24 h period.

^{1}H and ^{31}P NMR Spectroscopy. ^{1}H and ^{31}P NMR spectra were recorded at 25 °C using a Bruker 400 MHz Avance III NMR spectrometer operating at 400.16 MHz for the ^{1}H frequency and 161.57 MHz for the ^{31}P frequency, respectively. The reported hydrogen shifts are relative to CH_2Cl_2 (residual solvent peak) at δ 5.32 ppm, and phosphorus chemical shifts are relative to phosphoric acid (in a glass capillary; δ 0.00 ppm).

X-ray Photoelectron Spectroscopy. **1** and **2** were analyzed by XPS, and the data recorded are present in the Supporting Information. A PHI 5000 Versaprobe spectrometer was used to record the XPS data. The system is equipped with a monochromatic Al Kα X-ray source (Al Kα = 1486.6 eV). The specific details of the XPS study are similar to those of other XPS studies reported from our laboratory.[98−101] The XPS data was analyzed using Multipak version 9.7c computer software,[102] and by applying Gaussian−Lorentz fits (the Gaussian/Lorentz ratios were always >95%).

Matrix-Assisted Laser Desorption Ionization−Time of Flight (MALDI−TOF) Spectrometry. MALDI−TOF spectra were collected using a Bruker Microflex LRF20 in the positive mode with the minimum laser power required to observe signals, utilizing anthracene as matrix.

Electrochemical Characterization. *Electrochemical Analysis.* The electrochemical properties of 0.8 mM solutions of the Grubbs first (**1**) and second (**2**) generation catalysts were measured in dry CH_2Cl_2 containing 0.08 M tetrabutylammonium hexafluorophosphate, $[N(^nBu)_4][PF_6]$, as supporting electrolyte. The experiments were conducted under a blanket of argon at both 5 and 25 °C, utilizing a BAS 100 B/W electrochemical workstation interfaced with a personal computer. A three-electrode cell was used, utilizing a Pt auxiliary electrode, a glassy carbon working electrode with a surface area of 3.14 mm^2, and a Pt reference electrode. The working electrode was polished on a Buhler polishing mat, utilizing a 1 μm—and then a 1/4 μm—diamond paste. Consecutive experiments under the same experimental conditions showed that all formal reduction and oxidation potentials were reproducible within 5 mV. Experimental potentials were measured against the Pt reference electrode, but the results presented are referenced against the ferrocene couple, FcH/FcH^+, as an internal standard, as suggested by IUPAC.[103] However, the FcH/FcH^+ couple interfered with the oxidation wave of the Grubbs complexes; thus, decamethylferrocene (FcH*) was used as an internal standard and referenced back to ferrocene. We found that under our conditions $E^{\circ}_{Fc^*}{}' = -545$ mV *vs* FcH/FcH^+.

ASSOCIATED CONTENT

Supporting Information

The Supporting Information is available free of charge at https://pubs.acs.org/doi/10.1021/acsomega.1c03109.

The ATR−FTIR graphs, additional ^{1}H and ^{31}P NMR spectra, MALDI−TOF MS, and CVs figures (PDF)

AUTHOR INFORMATION

Corresponding Author

Elizabeth Erasmus − *Department of Chemistry, University of the Free State, Bloemfontein 9300, South Africa;* orcid.org/0000-0003-0546-697X; Phone: 27 51 4019656; Email: Erasmus@ufs.ac.za; Fax: 27 51 4017295

Authors

Marthinus R. Swart − *Department of Chemistry, University of the Free State, Bloemfontein 9300, South Africa*

Charlene Marais − *Department of Chemistry, University of the Free State, Bloemfontein 9300, South Africa;* orcid.org/0000-0003-3846-1956

Complete contact information is available at: https://pubs.acs.org/10.1021/acsomega.1c03109

Notes

The authors declare no competing financial interest.

ACKNOWLEDGMENTS

The South African National Research Foundation is acknowledged for their financial support with grants 118076 (C.M.) and 119028 (E.E.). Sasol and the Central Research Fund of the University of the Free State, Bloemfontein, South Africa, are also acknowledged for financial support.

ADDITIONAL NOTE

[i] % PCy_3 dissociation was determined as follows: $$\%PCy_3 \text{ dissociation} = \frac{\int O = PCy_3}{\int O = PCy_3 + \int \mathbf{1} \text{ or } \mathbf{2}} \times 100.$$

REFERENCES

(1) Nguyen, S. T.; Johnson, L. K.; Grubbs, R. H.; Ziller, J. W. Ring-Opening Metathesis Polymerization (ROMP) Of Norbornene By A Group VIII Carbene Complex In Protic Media. *J. Am. Chem. Soc.* **1992**, *114*, 3974−3975.

(2) Singh, O. M. Metathesis Catalysts: Historical Perspective, Resent Developments And Practical Applications. *J. Sci. Ind. Res.* **2006**, *65*, 957−965.

(3) Trnka, T. M.; Grubbs, R. H. The Development Of L_2X_2Ru=CHR Olefin Metathesis Catalysts: An Organometallic Success Story. *Acc. Chem. Res.* **2001**, *34*, 18−29.

(4) Grubbs, R. H. *Handbook of Metathesis*; Wiley-VCH, 2003; Vol. *2*.

(5) Herndon, J. W. The Chemistry Of The Carbon−Transition Metal Double And Triple Bond: Annual Survey Covering The Year 2018. *Coord. Chem. Rev.* **2019**, No. 213051.

(6) Mol, J. C. Application Of Olefin Metathesis In Oleochemistry: An Example Of Green Chemistry. *Green Chem.* **2002**, *4*, 5−13.

(7) Ogba, O. M.; Warner, N. C.; O'Leary, D. J.; Grubbs, R. H. Recent Advances In Ruthenium-Based Olefin Metathesis. *Chem. Soc. Rev.* **2018**, *47*, 4510−4544.

(8) Liu, P.; Ai, C. Olefin Metathesis Reaction In Rubber Chemistry And Industry And Beyond. *Ind. Eng. Chem. Res.* **2018**, *57*, 3807−3820.

(9) Yang, Q.; Alper, H.; Xiao, W.-J. Efficient Method For The Synthesis Of Chiral Pyrrolidine Derivatives Via Ring-Closing Enyne Metathesis Reaction. *Org. Lett.* **2007**, *9*, 769−771.

(10) Schmidt, B.; Staude, L. Ring-Size-Selective Enyne Metathesis As A Tool For Desymmetrization Of An Enantiopure C_2-Symmetric Building Block. *J. Org. Chem.* **2009**, *74*, 9237−9240.

(11) Keitz, B. K.; Grubbs, R. H. Ruthenium Olefin Metathesis Catalysts Bearing Carbohydrate-Based *N*-Heterocyclic Carbenes. *Organometallics* **2010**, *29*, 403−408.

(12) Yelchuri, V.; Srikanth, K.; Prasad, R. B. N.; Karuna, M. S. L. Olefin Metathesis Of Fatty Acids And Vegetable Oils. *J. Chem. Sci.* **2019**, *131*, 1−16.

(13) Mouawia, A.; Nourry, A.; Gaumont, A.-C.; Pilard, J.-F.; Dez, I. Controlled Metathetic Depolymerization Of Natural Rubber In Ionic Liquids: From Waste Tires To Telechelic Polyisoprene Oligomers. *ACS Sustainable Chem. Eng.* **2017**, *5*, 696−700.

(14) Eleutrio, H. S. Metal Catalyzed Polymerization of Cyclic Olefins. U.S. Patent US30749181963.

(15) Banks, R. L.; Bailey, G. C. Olefin Disproportionation. A New Catalytic Process. *Ind. Eng. Chem. Prod. Res. Dev.* **1964**, *3*, 170−173.

(16) Chauvin, Y. Olefin Metathesis: The Early Days (Nobel Lecture). *Angew. Chem., Int. Ed.* **2006**, *45*, 3740−3765.

(17) Fischer, E. O.; Maasböl, A. On The Existence Of A Tungsten Carbonyl Carbene Complex. *Angew. Chem., Int. Ed.* **1964**, *3*, 580−581.

(18) Astruc, D. The Metathesis Reactions: From A Historical Perspective To Recent Developments. *New J. Chem.* **2005**, *29*, 42−56.

(19) Schrock, R. R. An "Alkylcarbene" Complex Of Tantalum By Intramolecular α-Hydrogen Abstraction. *J. Am. Chem. Soc.* **1974**, *96*, 6796−6797.

(20) Wengrovius, J. H.; Schrock, R. R.; Churchill, M. R.; Missert, J. R.; Youngs, W. J. Tungsten-oxo Alkylidene Complexes As Olefins Metathesis Catalysts And The Crystal Structure of $W(O)(CHCMe_3)(PEt_3)Cl_2$. *J. Am. Chem. Soc.* **1980**, *102*, 4515−4516.

(21) Wu, Z.; Nguyen, S. T.; Grubbs, R. H.; Ziller, J. W. Reactions Of Ruthenium Carbenes Of The Type $(PPh_3)_2(X)_2Ru$=CH−CH=CPh_2 (X = Cl and CF_3COO) With Strained Acyclic Olefins And Functionalized Olefins. *J. Am. Chem. Soc.* **1995**, *117*, 5503−5511.

(22) Novak, B. M.; Grubbs, R. H. Catalytic Organometallic Chemistry In Water: The Aqueous Ring-Opening Metathesis Polymerization Of 7-Oxanorbornene Derivatives. *J. Am. Chem. Soc.* **1988**, *110*, 7542−7453.

(23) Grubbs, R. H. Olefin-Metathesis Catalysts For The Preparation Of Molecules And Materials (Nobel Lecture). *Angew. Chem., Int. Ed.* **2006**, *45*, 3760−3765.

(24) Wilhelm, T. E.; Belderrain, T. R.; Brown, S. N.; Grubbs, R. H. Reactivity Of $Ru(H)(H_2)Cl(PCy_3)_2$ With Propargyl And Vinyl Chlorides: New Methodology To Give Metathesis-Active Ruthenium Carbenes. *Organometallics* **1997**, *16*, 3867−3869.

(25) Schwab, P.; Grubbs, R. H.; Ziller, J. W. Synthesis And Applications Of $RuCl_2$(=CHR′)$(PR_3)_2$: The Influence Of The Alkylidene Moiety On Metathesis Activity. *J. Am. Chem. Soc.* **1996**, *118*, 100−110.

(26) Jarzembska, K.; Seal, S.; Woźniak, K.; Szadkowska, A.; Bieniek, M.; Grela, K. X-Ray Photoelectron Spectroscopy and Reactivity Studies Of A Series Of Ruthenium Catalysts. *ChemCatChem* **2009**, *1*, 144−151.

(27) Lane, D. R.; Beaver, C. M.; Olmstead, M. M.; Schore, N. E. Steric and Electronic Effects of Carbene Substitution in Grubbs First-Generation Catalysts. *Organometallics* **2009**, *28*, 6789−6797.

(28) Grela, K.; Harutyunyan, S.; Michrowska, A. A Highly Efficient Ruthenium Catalyst For Metathesis Reactions. *Angew. Chem., Int. Ed.* **2002**, *41*, 4038−4040.

(29) Love, J. A.; Sanford, M. S.; Day, M. W.; Grubbs, R. H. Synthesis, Structure, and Activity of Enhanced Initiators for Olefin Metathesis. *J. Am. Chem. Soc.* **2003**, *125*, 10103−10109.

(30) Scholl, M.; Ding, S.; Lee, C. W.; Grubbs, R. H. Synthesis And Activity Of A New Generation Of Ruthenium-Based Olefin Metathesis Catalysts Coordinated With 1,3-Dimesityl-4,5-dihydroimidazol-2-ylidene Ligands. *Org. Lett.* **1999**, *1*, 953−956.

(31) Scholl, M.; Trnka, T. M.; Morgan, J. P.; Grubbs, R. H. Increased Ring Closing Metathesis Activity Of Ruthenium-Based Olefin Metathesis Catalysts Coordinated With Imidazolin-2-ylidene Ligands. *Tetrahedron Lett.* **1999**, *40*, 2247−2250.

(32) J., Cossy *Synthesis of Saturated Oxygenated Heterocycles II*; Springer, 2014; pp 323−324.

(33) Huang, J.; Stevens, E. D.; Nolan, S. P.; Petersen, J. L. Olefin Metathesis-Active Ruthenium Complexes Bearing A Nucleophilic Carbene Ligand. *J. Am. Chem. Soc.* **1999**, *121*, 2674−2678.

(34) Huang, J.; Schanz, H.-J.; Stevens, E. D.; Nolan, S. P. Stereoelectronic Effects Characterizing Nucleophilic Carbene Ligands Bound To The Cp*RuCl (Cp* = H^5-C_5Me_5) Moiety: A Structural And Thermochemical Investigation. *Organometallics* **1999**, *18*, 2370−2375.

(35) Lummiss, J. A. M.; Higman, C. S.; Fyson, D. L.; McDonald, R.; Fogg, D. E. The Divergent Effects Of Strong NHC Donation In Catalysis. *Chem. Sci.* **2015**, *6*, 6739−6746.

(36) Leuthäußer, S.; Schmidts, V.; Thiele, C. M.; Plenio, H. Π-Face Donor Properties Of *N*-Heterocyclic Carbenes In Grubbs II Complexes. *Chem. − Eur. J.* **2008**, *14*, 5465−5481.

(37) Swart, M. R.; Twigge, L.; Marais, C.; Bezuidenhoudt, B. C. B. A Variable Temperature NMR Analysis And Resonance Assignment Of The Grubbs Second Generation Catalyst. *Polyhedron* **2018**, *152*, 31−36.

(38) Olszewski, T. K.; Bieniek, M.; Skowerski, K.; Grela, K. A New Tool In The Toolbox: Electron-Withdrawing Group Activated Ruthenium Catalysts For Olefin Metathesis. *Synlett* **2013**, *24*, 903−919.

(39) Al-Hashimi, M.; Hongfa, C.; George, B.; Bazzi, H. S.; Bergbreiter, D. E. A Phase-Separable Second-Generation Hoveyda-Grubbs Catalyst For Ring-Opening Metathesis Polymerization. *J. Polym. Sci., Part A: Polym. Chem.* **2012**, *50*, 3954−3956.

(40) Briot, A.; Bujard, M.; Gouverneur, V.; Nolan, S. P.; Mioskowski, C. Improvement In Olefin Metathesis Using A New Generation Of Ruthenium Catalyst Bearing An Imidazolylidene Ligand: Synthesis Of Heterocycles. *Org. Lett.* **2000**, *2*, 1517−1519.

(41) Bailey, G. A.; Lummiss, J. A. M.; Foscato, M.; Occhipinti, G.; McDonald, R.; Jensen, V. R.; Fogg, D. E. Decomposition Of Olefin Metathesis Catalysts By Brønsted Base: Metallacyclobutane Deprotonation As A Primary Deactivating Event. *J. Am. Chem. Soc.* **2017**, *139*, 16446−16449.

(42) Santos, A. G.; Bailey, G. A.; dos Santos, E. N.; Fogg, D. E. Overcoming Catalyst Decomposition In Acrylate Metathesis:

https://doi.org/10.1021/acsomega.1c03109
ACS Omega 2021, 6, 28642−28653

Polyphenol Resins As Enabling Agents For PCy_3-Stabilized Metathesis Catalysts. *ACS Catal* **2017**, *7*, 3181−3189.
(43) Marx, F. T. I.; Jordaan, J. H. L.; Lachmann, G.; Vosloo, H. C. M. A Molecular Modeling Study Of The Changes Of Some Steric Properties Of The Precatalysts During The Olefin Metathesis Reaction. *J. Comput. Chem.* **2014**, *35*, 1457−1463.
(44) Vummaleti, S. V. C.; Cavallo, L.; Poater, A. The Driving Force Role Of Ruthenacyclobutanes. *Theor. Chem. Acc.* **2015**, *134*, 22.
(45) Minenkov, Y.; Occhipinti, G.; Jensen, V. R. Complete Reaction Pathway Of Ruthenium-Catalyzed Olefin Metathesis Of Ethyl Vinyl Ether: Kinetics And Mechanistic Insight From DFT. *Organometallics* **2013**, *32*, 2099−2111.
(46) Forman, G. S.; McConnell, A. E.; Tooze, R. P.; Janse van Rensburg, W.; Meyer, W. H.; Kirk, M. M.; Dwyer, C. L.; Serfontein, D. A. A Convenient System For Improving The Efficiency Of First-Generation Ruthenium Olefin Metathesis Catalysts. *Organometallics* **2005**, *24*, 4528−4542.
(47) Occhipinti, G.; Koudriavtsev, V.; Törnroos, K. W.; Jensen, V. R. Theory-Assisted Development Of A Robust And Z-Selective Olefin Metathesis Catalyst. *Dalton Trans.* **2014**, *43*, 11106−11117.
(48) Kvíčala, J.; Schindler, M.; Kelbichová, V.; Babuněk, M.; Rybáčková, M.; Kvíčalová, M.; Cvačka, J.; Březinová, A. experimental and theoretical study of hoveyda−grubbs catalysts modified by perfluorohexyl ponytail in the alkoxybenzylidene ligand. *J. Fluorine Chem.* **2013**, *153*, 12−25.
(49) Kajetanowicz, A.; Grela, K. Nitro And Other Electron Withdrawing Group Activated Ruthenium Catalysts For Olefin Metathesis Reactions. *Angew. Chem., Int. Ed.* **2021**, *60*, 13738−13756.
(50) Eivgi, O.; Vaisman, A.; Lemcoff, N. G. Latent, Yet Highly Active Photoswitchable Olefin Metathesis Precatalysts Bearing Cyclic Alkyl Amino Carbene (CAAC)/Phosphite Ligands. *ACS Catal.* **2021**, *11*, 703−709.
(51) Kumandin, P. A.; Antonova, A. S.; Alekseeva, K. A.; Nikitina, E. V.; Novikov, R. A.; Vasilyev, K. A.; Sinelshchikova, A. A.; Grigoriev, M. S.; Polyanskii, K. B.; Zubkov, F. I. Influence Of The N→Ru Coordinate Bond Length On The Activity Of New Types Of Hoveyda−Grubbs Olefin Metathesis Catalysts Containing A Six-Membered Chelate Ring Possessing A Ruthenium−Nitrogen Bond. *Organometallics* **2020**, *39*, 4599−4607.
(52) Xu, Y.; Wong, J. J.; Samkian, A. E.; Ko, J. H.; Chen, S.; Houk, K. N.; Grubbs, R. H. Efficient *Z*-Selective Olefin-Acrylamide Cross-Metathesis Enabled By Sterically Demanding Cyclometalated Ruthenium Catalysts. *J. Am. Chem. Soc.* **2020**, *142*, 20987−20993.
(53) Swart, M. R.; Twigge, L.; Marais, C.; Erasmus, E.; Bezuidenhoudt, B. C. B. Olefin Metathesis, *p*-Cresol, And The Second Generation Grubbs Catalyst: Fitting The Pieces. *Eur. J. Inorg. Chem.* **2021**, *2021*, 1752−1762.
(54) Kim, Y.; Chen, C. H.; Hilty, C. Direct Observation Of Ru-Alkylidene Forming Into Ethylene In Ring-Closing Metathesis From Hyperpolarized ^{1}H NMR. *Chem. Commun.* **2018**, *54*, 4333−4336.
(55) Easter, Q. T.; Blum, S. A. Kinetics Of The Same Reaction Monitored Over Nine Orders Of Magnitude In Concentration: When Are Unique Subensemble And Single-Turnover Reactivity Displayed? *Angew. Chem., Int. Ed.* **2018**, *57*, 12027−12032.
(56) Silva Elipe, M. V.; Cherney, A.; Krull, R.; Donovan, N.; Tedrow, J.; Pooke, D.; Colson, K. L. Application of the New 400 MHz High-Temperature Superconducting (HTS) Power-Driven Magnet NMR Technology For Online Reaction Monitoring: Proof Of Concept With A Ring-Closing Metathesis (RCM) Reaction. *Org. Process Res. Dev.* **2020**, *24*, 1428−1434.
(57) Gordon, C. P.; Raynaud, C.; Andersen, R. A.; Copéret, C.; Eisenstein, O. Carbon-13 NMR Chemical Shift: A Descriptor For Electronic Structure And Reactivity Of Organometallic Compounds. *Acc. Chem. Res.* **2019**, *52*, 2278−2289.
(58) Maishal, T. K.; Mondal, B.; Puranik, V. G.; Wadgaonkar, P. P.; Lahiri, G. K.; Sarkar, A. Synthesis, Structure, Electrochemistry And ROMP-Activity Of New Ferrocenyl Analog Of Grubbs' Metathesis Catalyst. *J. Organomet. Chem.* **2005**, *690*, 1018−1027.
(59) Akkoç, M.; Öz, E.; Demirel, S.; Dorcet, V.; Roisnel, T.; Bayri, A.; Bruneau, C.; Altin, S.; Yaşar, S.; Özdemir, I. Investigation Of Potential Hybrid Capacitor Property Of Chelated N-Heterocyclic Carbene Ruthenium(II) Complex. *J. Organomet. Chem.* **2018**, *866*, 214−222.
(60) Ramesh, M.; Kumar, M. D.; Jaccob, M.; Therrien, B.; Venkatachalam, G. Cyclometalated Ruthenium(II) Carbonyl Complexes Containing 2-(Biphenylazo)phenolate Ligands: Synthesis, Structure, DFT Study And Catalytic Activity Towards Oxidation And Transfer Hydrogenation. *Inorg. Chim. Acta* **2018**, *477*, 40−50.
(61) Maity, L.; Adhikary, S. D.; Mondal, A.; Kisan, H. K.; Isab, A. A.; Goswami, S.; Dinda, J. Synthesis, Structure, Theoretical Studies And Electrochemistry Of Ru(II)−*N* Heterocyclic Carbenes. *Inorg. Chim. Acta* **2018**, *479*, 141−147.
(62) Labande, A.; Daran, J.-C.; Long, N. J.; White, A. J. P.; Poli, R. Rhodium(III) And Ruthenium(II) Complexes Of Redox-Active, Chelating *N*-Heterocyclic Carbene/Thioether Ligands. *New J. Chem.* **2011**, *35*, 2162−2168.
(63) Wang, G.-F.; Chen, F.; Liu, Y.-Z.; Chen, X.-T.; Xue, Z.-L. Synthesis And Structural Characterization Of Ruthenium(II) Carbonyl Complexes With A Bistriazole *N*-Heterocyclic Carbene Ligand. *Inorg. Chim. Acta* **2012**, *386*, 46−49.
(64) Merino, E.; Poli, E.; Díaz, U.; Brunel, D. Synthesis And Characterization Of New Ruthenium *N*-Heterocyclic Carbene Hoveyda II-Type Complexes. Study Of Reactivity In Ring Closing Metathesis Reactions. *Dalton Trans.* **2012**, *41*, 10913−10918.
(65) Nelson, D. J.; Manzini, S.; Urbina-Blanco, C. A.; Nolan, S. P. Key Processes In Ruthenium-Catalysed Olefin Metathesis. *Chem. Commun.* **2014**, *50*, 10355−10375.
(66) Afonso, M. B. A.; Gonçalves, L. G.; Borim, P.; Sá, J. L. S.; Goi, B. E.; Carvalho-Jr, V. P. Atom Transfer Radical Polymerization Of Methyl Methacrylate Mediated By Grubbs 1st And 2nd Generation Catalysts: Insight Into The Active Species. *J. Braz. Chem. Soc.* **2017**, *28*, 1407−1413.
(67) Forcina, V.; García-Domínguez, A.; Lloyd-Jones, G. C. Kinetics Of Initiation Of The Third Generation Grubbs Metathesis Catalyst: Convergent Associative And Dissociative Pathways. *Faraday Discuss.* **2019**, *220*, 179−195.
(68) Matsuo, T.; Yoshida, T.; Fujii, A.; Kawahara, K.; Hirota, S. Effect Of Added Salt On Ring-Closing Metathesis Catalyzed By A Water-Soluble Hoveyda−Grubbs Type Complex To Form *N*-Containing Heterocycles In Aqueous Media. *Organometallics* **2013**, *32*, 5313−5319.
(69) Wilson, G. O.; Porter, K. A.; Weissman, H.; White, S. R.; Sottos, N. R.; Moore, J. S. Stability Of Second Generation Grubbs' Alkylidenes To Primary Amines: Formation Of Novel Ruthenium-Amine Complexes. *Adv. Synth. Catal.* **2009**, *351*, 1817−1825.
(70) Swart, M. R.; Bezuidenhoudt, B. C. B.; Marais, C.; Erasmus, E. Spectroscopic Characterisation Of Grubbs 2nd Generation Catalyst And Its *p*-Cresol Derivatives. *Inorg. Chim. Acta* **2021**, *514*, No. 120001.
(71) Harris, D.; Bertolucci, M. *Symmetry and Spectroscopy. An Introduction to Vibrational and Electronic Spectroscopy*; Dover Publications, Inc.: New York, 1989.
(72) Griffiths, J. R.; Keister, J. B.; Diver, S. T. From Resting State To The Steady State: Mechanistic Studies Of Ene−Yne Metathesis Promoted By The Hoveyda Complex. *J. Am. Chem. Soc.* **2016**, *138*, 5380−5391.
(73) Sanford, M. S.; Love, J. A.; Grubbs, R. H. Mechanism And Activity Of Ruthenium Olefin Metathesis Catalysts. *J. Am. Chem. Soc.* **2001**, *123*, 6543−6554.
(74) Jawiczuk, M.; Marczyk, A.; Trzaskowski, B. Decomposition of Ruthenium Olefin Metathesis Catalyst. *Catalysts* **2020**, *10*, 887.
(75) Kirk, M. M. Ruthenium Based Homogeneous Olefin Metathesis. M.Sc. Dissertation, University of the Free State: Bloemfontein, South Africa, 2005.
(76) Gallagher, M. M.; Rooney, A. D.; Rooney, J. J. Variable Temperature ^{1}H NMR Studies on Grubbs Catalysts. *J. Organomet. Chem.* **2008**, *693*, 1252−1260.

https://doi.org/10.1021/acsomega.1c03109
ACS Omega 2021, 6, 28642−28653

(77) Sauvage, X.; Demonceau, A.; Delaude, L. Imidazol(in)ium-2-carboxylates As *N*-Heterocyclic Carbene Precursors For The Synthesis Of Second Generation Ruthenium Metathesis Catalysts. *Adv. Synth. Catal.* **2009**, *351*, 2031−2038.
(78) Schraml, J.; Čapka, M.; Blechta, V. ^{31}P And ^{13}C NMR Spectra Of Cyclohexylphenylphosphines, Tricyclohexylphosphine And Triphenylphosphine. *Magn. Reson. Chem.* **1992**, *30*, 544−547.
(79) Bresó-Femenia, E.; Godard, C.; Claver, C. S.; et al. Selective Catalytic Deuteration Of Phosphorus Ligands Using Ruthenium Nanoparticles: A New Approach To Gain Information On Ligand Coordination. *Chem. Commun.* **2015**, *51*, 16342−16345.
(80) Dinger, M. B.; Mol, J. C. Degradation of the First-Generation Grubbs Metathesis Catalyst with Primary Alcohols, Water, and Oxygen. Formation and Catalytic Activity of Ruthenium(II) Monocarbonyl Species. *Organometallics* **2003**, *22*, 1089−1095.
(81) van der Westhuizen, H. J.; Roodt, A.; Meijboom, R. Kinetics of thermal decomposition and of the reaction with oxygen, ethene and 1-octene of first generation Grubbs' catalyst precursor. *Polyhedron* **2010**, *29*, 2776−2779.
(82) Higman, C. S.; Rufh, S. A.; McDonald, R.; Fogg, D. E. Synthesis And Dynamic Behaviour Of A Dimeric Ruthenium Benzylidene Complex Bearing A Truncated N-Heterocyclic Carbene Ligand. *J. Organomet. Chem.* **2017**, *847*, 162−166.
(83) Amoroso, D.; Yap, G. P. A.; Fogg, D. E. Deactivation Of Ruthenium Metathesis Catalysts Via Facile Formation Of Face-Bridged Dimers. *Organometallics* **2002**, *21*, 3335−3343.
(84) Amoroso, D.; Snelgrove, J. L.; Conrad, J. C.; Drouin, S. D.; Yap, G. P. A.; Fogg, D. E. An Attractive Route To Olefin Metathesis Catalysts: Facile Synthesis Of A Ruthenium Alkylidene Complex Containing Labile Phosphane Donors. *Adv. Synth. Catal.* **2002**, *344*, 757−763.
(85) Wolf, W. J.; Lin, T.-P.; Grubbs, R. H. Examining The Effects Of Monomer And Catalyst Structure On The Mechanism Of Ruthenium-Catalyzed Ring-Opening Metathesis Polymerization. *J. Am. Chem. Soc.* **2019**, *141*, 17796−177808.
(86) Gericke, H. J.; Barnard, N. I.; Erasmus, E.; Swarts, J. C.; Cook, M. J.; Aquino, M. A. S. Solvent And Electrolyte Effects In Enhancing The Identification Of Intramolecular Electronic Communication In A Multi Redox-Active Diruthenium Tetraferrocenoate Complex, A Triple-Sandwiched Dicadmium Phthalocyanine And A Ruthenocene-Containing β-Diketone. *Inorg. Chim. Acta* **2010**, *363*, 2222−2232.
(87) Erasmus, E.; Conradie, J.; Muller, A.; Swarts, J. C. Synthesis, Crystal Structure And Electrochemistry Of Tetrahedral Mono-B-Diketonato Titanocenyl Complexes. *Inorg. Chim. Acta* **2007**, *360*, 2277−2283.
(88) Zanello, P.; Nervi, C.; de Biani, F. F. *Inorganic Electrochemistry: Theory, Practice and Application*, 2nd ed.; The Royal Chemical Society: Cambridge, 2012.
(89) Elgrishi, N.; Rountree, K. J.; McCarthy, B. D.; Rountree, E. S.; Eisenhart, T. T.; Dempsey, J. L. A Practical Beginner's Guide to Cyclic Voltammetry. *J. Chem. Educ.* **2018**, *95*, 197−206.
(90) Erasmus, E.; Swarts, J. C. Intramolecular communication And Electrochemical Observation Of The 17-Electron Ruthenocenium Cation In Fluorinated Ruthenocene-Containing β-Diketones; Polymorphism Of $C_{10}H_{21}$ And $C_{10}F_{21}$ Derivatives. *New J. Chem.* **2013**, *37*, 2862−2873.
(91) Trupia, S.; Nafady, A.; Geiger, W. E. Electrochemical Preparation Of The Bis(ruthenocenium) Dication. *Inorg. Chem.* **2003**, *42*, 5480−5482.
(92) Swarts, J. C.; Nafady, A.; Roudebush, J. H.; Trupia, S.; Geiger, W. E. One-Electron Oxidation Of Ruthenocene: Reactions Of The Ruthenocenium Ion In Gentle Electrolyte Media. *Inorg. Chem.* **2009**, *48*, 2156−2165.
(93) Kaifer, A. E.; Gomez-Kaifer, M. *Supramolecular Electrochemistry*, 1st ed.; Wiley-VCH: Weinheim, 1999; p 86.
(94) Fan, F.; Cai, C.; Li, J.; Zhang, P.; Li, G.; Li, C.; Yu, G.; et al. Microwave-assisted synthesis of glycopolymer by ring-opening metathess polymerization (ROMP) in an emulsion system. *Polym. Chem.* **2017**, *8*, 6709−6719.
(95) Matsuo, T.; Imai, C.; Yoshida, T.; Saito, T.; Hayashib, T.; Hirota, S. Creation of an artificial metalloprotein with a Hoveyda−Grubbs catalyst moiety through the intrinsic inhibition mechanism of a-chymotrypsin. *Chem. Commun.* **2012**, *48*, 1662−1664.
(96) Ton, S. J.; Fogg, D. E. The Impact of Oxygen on Leading and Emerging Ru-Carbene Catalysts for Olefin Metathesis: An Unanticipated Correlation Between Robustness and Metathesis Activity. *ACS Catal* **2019**, *9*, 11329−11334.
(97) Maishal, T. K.; Mondal, B.; Puranik, V. G.; Wadgaonkar, P. P.; Lahiri, G. K.; Amitabha, S. Synthesis, structure, electrochemistry and ROMP-activity of new ferrocenyl analog of Grubbs' metathesis catalyst. *J. Organomet. Chem.* **2005**, *690*, 1018−1027.
(98) Trzebiatowska-Gusowska, M.; Gągor, A.; Coetsee, E.; Erasmus, E.; Swart, H. C.; Swarts, J. C. Nano Islet Formation Of Formyl- And Carboxyferrocene, -Ruthenocene, -Osmocene And Cobaltocenium On Amine-Functionalized Silicon Wafers Highlighted By Crystallographic, AFM And XPS Studies. *J. Organomet. Chem.* **2013**, *745−746*, 393−403.
(99) van As, A.; Joubert, C. C.; Buitendach, B. E.; Erasmus, E.; Conradie, J.; Cammidge, A. N.; Chambrier, I.; Cook, M. J.; Swarts, J. C. Tetrabenzoporphyrin And -Mono-, -*Cis*-Di- And Tetrabenzotriazaporphyrin Derivatives: Electrochemical And Spectroscopic Implications Of Meso CH Group Replacement With Nitrogen. *Inorg. Chem.* **2015**, *54*, 5329−5341.
(100) Conradie, M. M.; Conradie, J.; Erasmus, E. Immobilisation Of Iron Tris(β-Diketonates) On A Two-Dimensional Flat Amine Functionalised Silicon Wafer: A Catalytic Study Of The Formation Of Urethane, From Ethanol And A Diisocyanate Derivative. *Polyhedron* **2014**, *79*, 52−59.
(101) van Rensburg, A. J.; Landman, M.; Erasmus, E.; van der Westhuizen, D.; Ferreira, H.; Conradie, M. M.; Conradie, J. Electrochemical And X-Ray Photoelectron Spectroscopic Insights Into Molybdenum(0) Fischer Ethoxycarbene Complexes. *Electrochim. Acta* **2016**, *219*, 204−213.
(102) Moulder, F.; Stickle, W. F.; Sobol, P. E.; Bomben, K. D. *Handbook of X-ray Photoelectron Spectroscopy*; ULVAC-PHI, Inc.: Enzo, Chigasaki, Japan, 1995.
(103) Gritzner, G.; Kůta, J. Recommendations on Reporting Electrode Potentials In Nonaqueous Solvents. *Pure Appl. Chem.* **1984**, *56*, 461−466.

https://doi.org/10.1021/acsomega.1c03109
ACS Omega 2021, 6, 28642−28653